

# Assessment of cross-type optical particle separation system

Kang Soo Lee · Sang Youl Yoon · Sang Bok Kim ·  
Kyung Heon Lee · Hyung Jin Sung ·  
Sang Soo Kim

Received: 8 November 2011 / Accepted: 4 January 2012 / Published online: 14 January 2012  
© Springer-Verlag 2012

**Abstract** This paper describes the optical and hydrodynamic characteristics of particle motion in a cross-type optical particle separator. The retention distance modulated by the optical force on a particle was measured in three dimensions for various vertical and horizontal positions via  $\mu$ -defocusing digital particle image velocimetry. The experimental data showed that the actual retention distance was smaller than the predicted retention distance under the assumption that the approaching velocity was constant through the cross-section of a microfluidic channel. The retention distance was shown to increase as the injection position of the particle shifted toward the channel side wall at a given vertical position due to a higher residence time within the region of influence of the laser beam. In contrast, the retention distance decreased as the injection position shifted toward the channel top/bottom walls at a given horizontal position. A theoretical modeling study was conducted to support and interpret the experimental measurements. The resolution of the particle separation procedure, which did not require adjusting the flow rate, laser power, or working fluid properties, was studied.

**Keywords** Cross-type optical particle separator · Retention distance · Scattering force · Gradient force · Poiseuille velocity field profile

## 1 Introduction

The techniques for particle and cell manipulation in a microfluidic channel are important in several research fields, including point-of-care diagnostics, life sciences, biological weapons detection, and drug discovery/screening, each of which field has its own needs (Gomez 2008). Many researchers have described particle/cell manipulation techniques in lab-on-a-chip-based microfluidic systems, such as electrophoretic, hydrodynamic, and magnetophoretic manipulation systems (Yamada et al. 2004; Mao et al. 2009; Ohshima and Kondo 1989; Pamme and Manz 2004). Optical particle manipulation techniques are one of the most well-developed particle manipulation methods, and have several advantages over other methods such as non-invasive nature, independence of the charge state of the particle and the surrounding medium, and requirements of relatively simple structures (Kim et al. 2008a; Kuhn et al. 2009).

The first approach to optical particle manipulation using a laser beam was carried out by Ashkin (1970). He demonstrated the optical acceleration and trapping of a glass microsphere suspended in water. Since then, many studies on optical particle manipulation have been reported, such as optical tweezer, optical chromatography, optical separation, etc. (Dholakia et al. 2008; Hart and Terray 2003; Ladavac et al. 2004; MacDonald et al. 2003; Wang et al. 2005; Yang et al. 2009; Hoi et al. 2009). Recently, a cross-type optical particle separator (COPS), which uses the scattering force to make a particle move across flow streamlines, was developed and characterized (Helmbrecht et al. 2007; Kim et al. 2006, 2008b; Hoi et al. 2010). When a particle flowing along the flow direction passes through a laser beam, the particle is displaced laterally due to the scattering force exerted perpendicular to the flow direction.

---

K. S. Lee · S. Y. Yoon · S. B. Kim · K. H. Lee ·  
H. J. Sung (✉) · S. S. Kim (✉)  
Department of Mechanical Engineering, KAIST,  
291 Daehak-ro, Yuseong-gu, Daejeon 305-701, Korea  
e-mail: hjsung@kaist.ac.kr

S. S. Kim  
e-mail: sskim@kaist.ac.kr

This lateral displacement is called the displacement distance or retention distance (Helmbrecht et al. 2007; Kim et al. 2006). The COPS has advantages, especially for cell separation, over other optical particle manipulation methods, e.g., optical tweezers, because it uses a loosely focused laser beam, minimizing the energy density, which can result in radiation-induced cell damage (Lee et al. 2011). The COPS configuration has wide applications in microfluidic platforms such as cell handling, particle ligand change, etc., as well as particle separation (Hsu et al. 2010; Hakem et al. 2010; Maruyama et al. 2011). The particle behavior during COPS was theoretically estimated and experimentally evaluated in terms of two factors: size and refractive index of the particle (Helmbrecht et al. 2007; Kim et al. 2006, 2008b). However, the effect of the flow velocity profile in a microfluidic channel was not considered in previous studies. Instead, they assumed that the approaching velocity was constant for simplicity. In a pressure-driven flow, Poiseuille flow with non-uniform velocity profile is constructed in the rectangular cross-section. Therefore, the previous approaches have validity only for the case of the particle motion at the tiny region of uniform velocity which is constructed at the center of the microfluidic channel.

For the applications of this system to actual devices, the particle behavior has to be determined with the flow velocity profile as well as the optical property. Hence, a technique to evaluate the particle behavior during COPS with the consideration of combined effect of the optical and hydrodynamic features is required. Because the retention distance is a function of the residence time in a laser beam, it varies according to the initial injection position of the particle. Hence, the particle behavior should be considered with the initial injection position in a cross-section and locally changed particle velocity due to the streamline shifts, as well as the particle size and refractive index.

In the present study, the effects of the optical and hydrodynamic features on a particle's behavior were studied. The retention distance of the particle as a function of the vertical and horizontal injection positions along a cross-section of the microfluidic channel were determined experimentally. A theoretical modeling study was conducted to support and help interpret the experimental data. These data were compared with results from a model that assumed a constant velocity profile. Because most microfluidic particle separation systems are influenced by the non-uniform velocity profile in a microfluidic channel, many researchers have described three-dimensional particle focusing methods using hydrodynamic or electric forces (Mao et al. 2009; Carlo et al. 2007; Chang et al. 2007; Kim and Yoo 2009; Tsai et al. 2008; Yu et al. 2005). However, most such techniques have concentrated on particle focusing at the center of a channel. Experimental and numerical

results suggested an improved method for manipulating the separation resolution without adjusting the parameters of flow rate, laser power, or working fluid properties.

To identify the three-dimensional position of a particle in a microfluidic channel, a three-dimensional particle tracking velocimetry (PTV) technique was employed. Although various PTV methods, such as particle diffraction- and confocal microscopy-based PTV methods, have been reported to track the trajectories of the particle in real-time, they revealed limitations in some applications: short analysis depth and slow particle scanning speed in the vertical direction (Kinoshita et al. 2007; Park and Kihm 2006; Wu et al. 2005). In the present study, the  $\mu$ -defocusing digital particle image velocimetry ( $\mu$ -DDPIV) technique was employed to permit simultaneous real-time particle tracking with fast particle tracking speed and long analysis depth (Yoon and Kim 2006).

## 2 Theory

Figure 1 shows a schematic diagram of a COPS system. The optical force that induces particle movement has two components: the scattering force acting in the direction of laser beam propagation and the gradient force acting in the direction of intensity gradient of laser beam. When a particle with a refractive index higher than that of the working fluid passes through a loosely focused laser beam ( $\omega_0 > \lambda$ , where  $\omega_0$  is the waist radius of the laser beam and  $\lambda$  is the wavelength of the laser beam), the particle is pushed in the direction of beam propagation by the scattering force if the absorption of the beam through the particle and working fluid is neglected. At the same time, the particle is accelerated/decelerated in the direction of the beam axis by the gradient force. As a result, particles are displaced perpendicular to the flow direction.

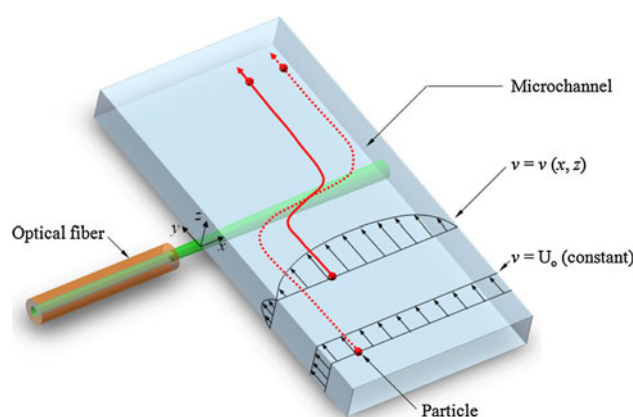


**Fig. 1** Schematic diagram of a cross-type optical particle separator and a description of the effects of the Poiseuille flow velocity field profile in a microfluidic channel

The behavior of a particle can be explained according to the following equations:

$$m_p \frac{du_p}{dt} + 6\pi\mu r_p u_p = F_s, \tag{1}$$

$$m_p \frac{dv_p}{dt} + 6\pi\mu r_p [v(x, z) - v_p] = F_g, \tag{2}$$

$$m_p \frac{dw_p}{dt} - 6\pi\mu r_p w_p = F_g, \tag{3}$$

where  $\mu$  is the dynamic viscosity of the working fluid,  $r_p$  is the radius of the particle,  $m_p$  is the particle mass, and  $v(x, z)$  is the y-directional fluid flow velocity.  $u_p$ ,  $v_p$ , and  $w_p$  are the x-, y-, and z-directional particle velocities, respectively.  $F_s$  and  $F_g$  are the scattering and gradient forces, respectively (Kim and Kim 2006),

$$F_s = \frac{n_1 r_p^2}{2c} \int_0^{2\pi} \int_0^{\pi/2} I(\rho, x) Q_s \sin 2\theta_1 d\theta_1 d\varphi, \tag{4}$$

$$F_g = \frac{n_1 r_p^2}{2c} \int_0^{2\pi} \int_0^{\pi/2} I(\rho, x) Q_g \sin 2\theta_1 \cos \varphi d\theta_1 d\varphi, \tag{5}$$

where  $n_1$  is the refractive index of the medium,  $c$  is the speed of light in free space,  $I(\rho, x)$  is the intensity distribution of illumination beam,  $\rho$  is the radial distance from the laser beam center axis to the center of the sphere, and  $Q_s$  and  $Q_g$  are dimensionless coefficients of the momentum change of photons in the scattering and gradient force directions, respectively.  $\theta_1$  is the angle between the incident photon and the particle surface, and  $\varphi$  is the polar angle.

In the previous studies of COPS system, the effect of the actual Poiseuille velocity profile in microfluidic channel was neglected, and the relation between the retention distance and the system parameters was derived under the assumption that  $v = U_o$  (constant). Instead, they measured the particle velocity from the experimentally acquired images and inserted the obtained particle velocity into the particle motion equation, given by Eqs. 1–3, to compare the experimental results with the theoretical predictions. However, since the retention distance can be affected by the vertical and horizontal position of a particle in real systems, the actual velocity profile should be considered. The Poiseuille velocity profile in a rectangular channel can be described using the following equation (Bruus 2008):

$$v(x, z) = \frac{4H^2 \Delta p}{\pi^3 \mu L} \sum_{n, \text{odd}} \frac{1}{n^3} \left[ 1 - \frac{\cosh\left(n\pi \frac{x-0.5W}{H}\right)}{\cosh\left(n\pi \frac{W}{2H}\right)} \right] \sin\left(n\pi \frac{z}{H}\right), \tag{6}$$

where  $\Delta p$  is the pressure drop,  $H$  is the height of the microfluidic channel, and  $W$  is the width of the channel.

For a rectangular microfluidic channel with  $H/W < 1$  and  $Re \lesssim 1,000$  ( $Re \equiv \rho U_o D_h / \mu$ , where  $\rho$  is the density of the working fluid,  $U_o$  is the mean fluid flow velocity in a microfluidic channel, and  $D_h$  is the hydraulic diameter of the microfluidic channel),  $\Delta p/L$  can be calculated as (Fuerstman et al. 2007):

$$\frac{\Delta p}{L} = \frac{a\mu Q}{WH^3}, \tag{7}$$

$$a = 12 \left[ 1 - \frac{192H}{\pi^5 W} \tanh\left(\frac{\pi W}{2H}\right) \right]^{-1}, \tag{8}$$

where  $Q$  is the fluid flow rate and  $a$  is a dimensionless parameter that depends on the aspect ratio of the rectangular channel.

### 3 Materials and methods

#### 3.1 $\mu$ -DDPIV method

The principle of  $\mu$ -defocusing digital particle image velocimetry ( $\mu$ -DDPIV) is illustrated in Fig. 2. A circular mask with three pinholes is placed between the objective lens and the image plane (a CMOS module). Each pinhole is located at the vertex of a triangle. When a target particle is positioned in the focusing plane of the objective lens, the three optical paths converge to a single point, and only one spot appears in the image plane. When a target particle is withdrawn from the focusing plane (defocused), however, the three optical paths diverge, and three distinct spots appear in the image plane at the vertices of a triangle. As the vertical distance between the object and the focusing plane increases, the distance between the two spots on image plane increases accordingly, and the size of the triangle increases. The inset of Fig. 2 shows the focused/defocused images at the image plane. The vertical position of the particle can be estimated from the circle that circumscribes the triangle formed by the three spot images. To calculate the distance from the bottom of the microfluidic channel to the target particle, a reference spot which has the same size of target particle is positioned at the bottom of the microfluidic channel (slide glass). Hence, the distance between the bottom of the microfluidic channel and the target particle can be estimated according to the size contrast between the circumscribed circles of the reference and target particle images. The vertical position with respect to the reference spot can be calculated according to the following equation (Yoon et al. 2011):

$$z - z_o = (\partial z / \partial D)(D - D_o), \tag{9}$$

where  $z$  and  $z_o$  are the vertical positions of the target particle and the reference spot, respectively.  $D$  and  $D_o$  are the

diameters of the circle circumscribing the target particle and the reference spot, respectively.  $\delta z/\delta D$  is the calibration coefficient, which represents the correlation between the vertical position and the observed image separation. The calibration coefficient which is affected by the refractive index of the working fluid can be calculated from the experimental piezo calibration (Yoon et al. 2011). While the transparent substrate, which has a spot with the same size as that of the target particle, is anchored to the piezo z-stage and shifted vertically ( $\Delta z$ ), the size change of the circumscribed circle ( $\Delta D$ ) is measured by varying the vertical position of the stage. A working fluid is introduced between the slide glass and the substrate.

### 3.2 Experimental setup

Figure 3 shows a schematic diagram of the experimental setup. A continuous wave neodymium-doped yttrium aluminum garnet (CW-Nd:YAG) laser ( $\lambda = 532$  nm,  $P_{CW} = 2$  W) was used to introduce the optical force and delivered into the microfluidic channel through a multimode glass optical fiber (MMJ-3I-IRVIS-50/125, NA = 0.22, OZ Optics Ltd.) to exert the optical force on particle. A microfluidic channel with a rectangular cross-section was fabricated by conventional soft lithography processes using polydimethylsiloxane (PDMS), due to its advantages, such as optical transparency and good optical properties (Psaltis et al. 2006). The PDMS device was bonded to a slide glass presenting a 5- $\mu$ m diameter reference spot. The width and height of the microfluidic channel were 300 and 100  $\mu$ m (aspect ratio, AR = 3), respectively. Polystyrene latex (PSL,  $n_o = 1.56$ , Duke Scientific Corp.) particles of diameter  $5.00 \pm 0.05$   $\mu$ m were used as the target particles. To prevent

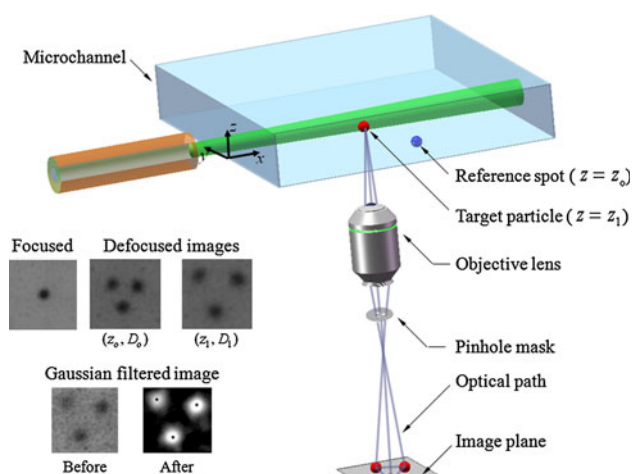


**Fig. 2** Operational principle of the  $\mu$ -DDPIV method: the insets show the defocused images at different  $z$ -positions and the Gaussian filtered image. Black dots in the Gaussian filtered images represent the three peak positions

attachment of the particles to the microfluidic channel wall, 2 wt% Pluronic F68 was added and de-ionized (DI) water was used (Lee et al. 2011). PSL particles suspended in DI water ( $n_1 = 1.33$ ) were fed to the microfluidic channel through a polytetrafluoroethylene (PTFE) tube, and the flow rates were adjusted using a syringe pump (Legato 200, KD Scientific). Images were collected using a 10-bit high-speed complementary metal-oxide semiconductor (CMOS) camera (pco. 1200 hs, PCO), and a white light emitting diode (LED) was adopted as the light source for the CMOS camera. A pinhole mask with a thickness of 0.2 mm was placed between the CMOS camera and the 20 $\times$  objective lens (LUCPlanFL N, Olympus Inc.). The interference filter (F10-632.8-4-2.00, CVI Optics) was used to block the scattered light of Nd-YAG laser beam. The particle trajectories were analyzed using an in-house image processing code programmed under C++ language. To estimate the calibration coefficient, a piezo z-stage with nanoscale resolution (TSGNF5/M, Thorlabs) was used.

## 4 Results and discussion

### 4.1 Experimental

The experiments were conducted using shadow imaging rather than fluorescence imaging with fluorescent particles, because these can reduce the power of the laser beam by absorption. Hence, the intensity profiles of images were reversed to locate the peak value. The noise was filtered from the experimental data, and the images were smoothed using a Gaussian spatial filter. The peak values were identified with sub-pixel accuracy, and a Gaussian peak fit was performed prior to computing the particle trajectories. After these processes, particle trajectories were evaluated using an in-house image processing routine.

Figure 4 shows a snapshot of a particle trajectory before Gaussian filtering. The mean flow velocity was  $U_o = 80$   $\mu$ m/s, the laser power at the fiber tip was  $P = 1.42$  W, and

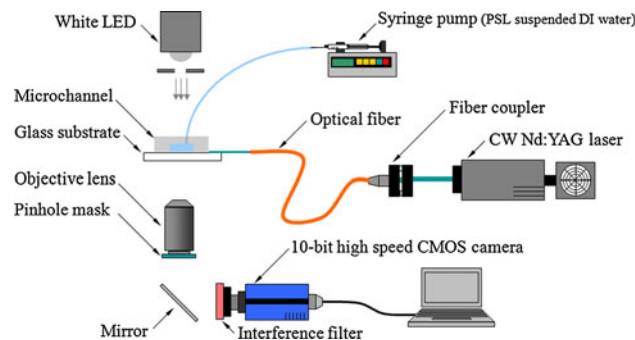


**Fig. 3** Schematic diagram of the experimental setup

the laser beam waist was  $2\omega_0 = 70 \mu\text{m}$ . The size difference between the circumscribed circles of the target particle and reference spot, which was patterned on the bottom of the microfluidic channel, permitted estimation of the initial vertical position relative to the bottom of the microfluidic channel. As seen in Fig. 4, when the particle flowed along the channel, it was displaced perpendicular to the direction of fluid flow by the optical force. The cell viability depends on the energy density ( $\text{W}/\text{cm}^2$ ), not the laser power itself ( $\text{W}$ ). In the present study, a loosely focused beam was used and the particle was not trapped but passed quickly ( $\sim 1 \text{ s}$ ) through the laser beam illumination region, while general optical trapping methods (e.g., optical tweezers) used a tightly focused beam during relatively long exposure times, i.e., the energy density of the present system is much lower than that of optical tweezers (Lee et al. 2011).

Figure 5 shows the piezo calibration curve from which the calibration coefficient was calculated. Because the calibration coefficient ( $\partial z/\partial D$ ) is affected by the refractive index of the working fluid, the system must be calibrated to determine the correlation between the image separation (size of the circumscribed circle) and the vertical position of the particle. The inverse of the calibration coefficient represents the measurement sensitivity (Yoon et al. 2011). In the present study, the calibration coefficient was  $2.0200 \pm 0.0010 \mu\text{m}/\text{pixel}$ . The coefficient of determination ( $R^2$ ) was 0.9992, which ensured a reasonable degree of precision in the regression line.

Figure 6a shows the experimental data corresponding to particle trajectories measured in three dimensions for particles injected into the microfluidic channel at different cross-sectional positions. The positions of the particles were not controlled artificially. Instead, the target particles were selected among the randomly inserted particles. We

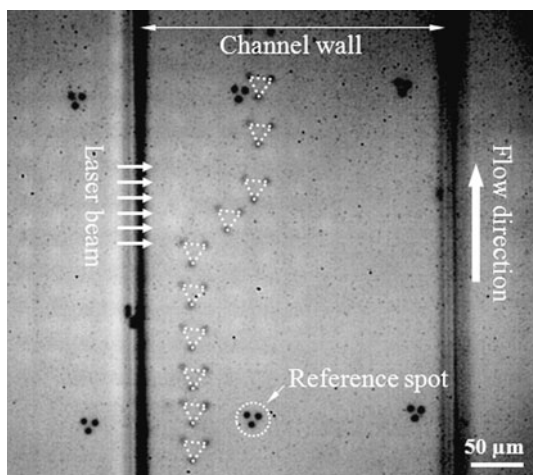


Fig. 4 Defocused image of the particle trajectories

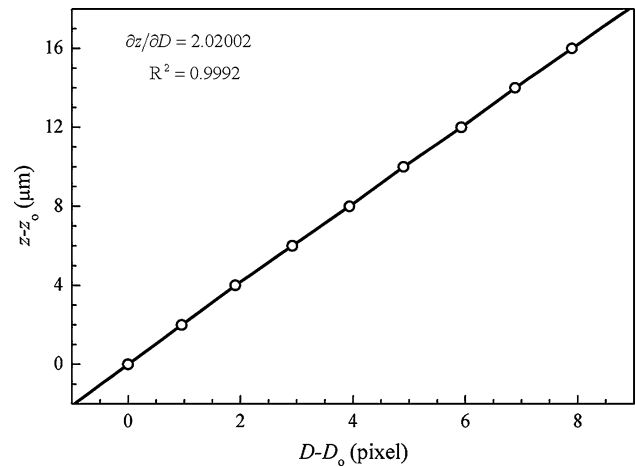
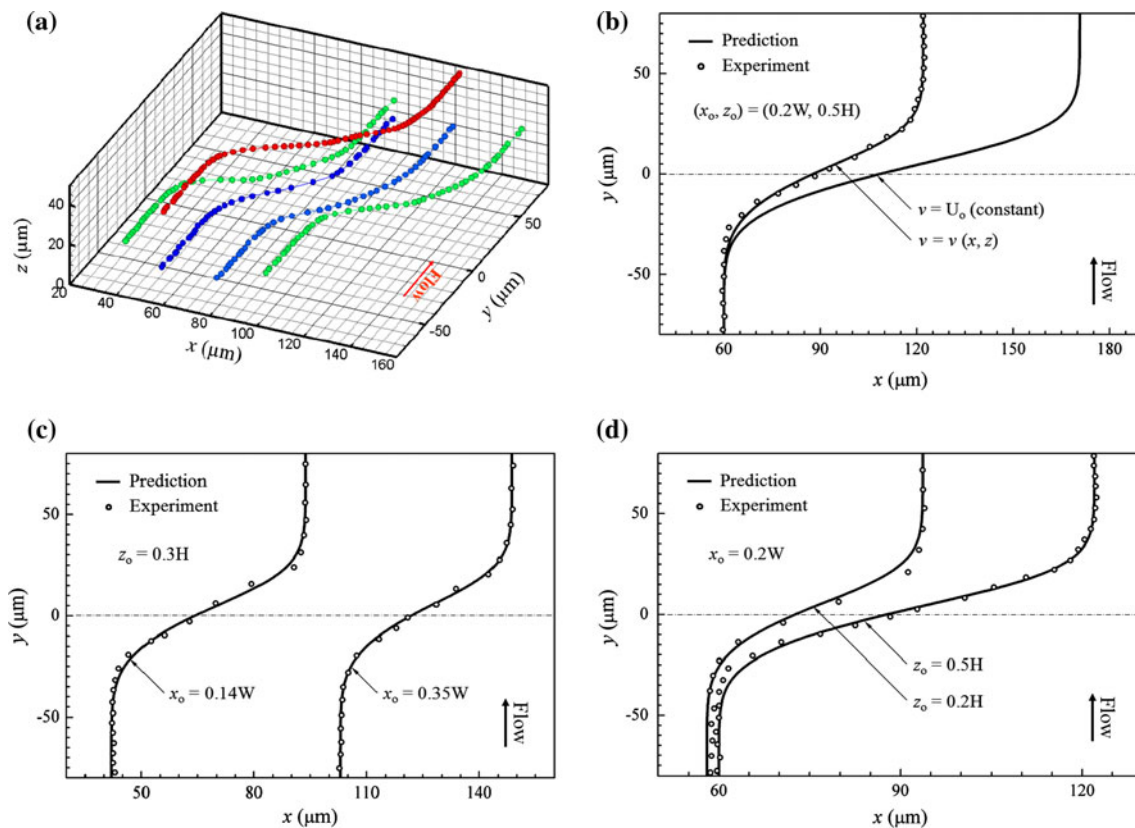


Fig. 5 Piezo calibration curve

analyzed 20 particles in the present study. The average ratio of the retention distance of the experiment to the prediction ( $\delta_{\text{experiment}}/\delta_{\text{prediction}} \times 100$ ) and the standard deviation were 103.3 and 7.6%, respectively. Among the data, particles with the same  $x$ - and different  $z$ -direction injection positions and particles with the same  $z$ - and different  $x$ -direction injection positions were chosen to account for the effects of the velocity profile and the radiation forces on the retention distance. The experimental conditions ( $U_0$ ,  $P$ , and  $2\omega_0$ ) were the same as those described in Fig. 4. The effect of the actual parabolic Poiseuille velocity profile on the particle separation behavior is shown in Fig. 6b. A particle was injected into the microfluidic channel at the initial position  $(x_0, z_0) = (0.2W, 0.5H)$ . As seen in Fig. 6b, the experimental trajectory was in excellent agreement with the theoretical predictions. The retention distance for the Poiseuille profile  $v = v(x, z)$  was a factor of two smaller than the distance obtained under the assumption  $v = U_0$  (constant). The actual local particle flow velocity was higher than the mean flow velocity, which reduced the residence time of the particle in the region of influence of the laser beam (Helmbrecht et al. 2007; Lee et al. 2011). Figure 6c shows two trajectories for particles injected at different  $x$ -positions and the same  $z$ -positions. The residence times in the laser beam differed because the local flow velocity depended on the particle position. The retention distances of the particles injected from the position  $(x_0, z_0) = (0.14W, 0.3H)$  and  $(x_0, z_0) = (0.35W, 0.3H)$  were 52 and 45  $\mu\text{m}$ , respectively. As the particle passed through the laser beam, it accelerated along the flow direction as it approached the laser beam axis (dash-dot line) and decelerated along the flow direction after it passed the laser beam axis due to the gradient force. Hence, the retention distance upstream of the laser beam axis was slightly smaller than that downstream of the laser beam axis, although the local flow velocity increased as the

particle was displaced toward the  $x$ -directional center axis of the microfluidic channel. These effects became more pronounced as the particle injection position shifted toward the  $x$ -directional center axis because the variations in the local velocity as a function of particle retention distance became smaller. As shown in Fig. 6c, the retention distances of particles injected at the positions  $(x_o, z_o) = (0.14W, 0.3H)$  and  $(x_o, z_o) = (0.35W, 0.3H)$  upstream of the laser beam axis were 23 and 18  $\mu\text{m}$ , respectively, whereas the retention distances downstream of the laser beam axis were 29 and 27  $\mu\text{m}$ , respectively. The trajectories for particles with two different  $z$ -positions but the same  $x$ -position are shown in Fig. 6d. The retention distances of the particles injected from the position  $(x_o, z_o) = (0.2W, 0.2H)$  and from the position  $(x_o, z_o) = (0.2W, 0.5H)$  were 35 and 60  $\mu\text{m}$ , respectively. Because the particle shifted in the  $z$ -direction away from the laser beam axis, the scattering force decreased rapidly and the gradient force increased. The retention distance is affected principally by the scattering force, so that it decreased along the  $z$ -position away from the laser beam axis.



**Fig. 6** Experimentally determined properties of the particle trajectories ( $\omega_o = 35 \mu\text{m}$ ,  $P = 1.42 \text{ W}$ ,  $d_p = 5 \mu\text{m}$ ,  $U_o = 80 \mu\text{m/s}$ ,  $AR = 3$ ). **a** Three-dimensional mapping of the retention distance of particles at different  $x$ - and  $z$ -directional injection positions. **b** Experimental measurements and theoretical predictions of the retention distance with consideration for the flow velocity field profile. The results calculated

## 4.2 Numerical

To broaden the analysis, numerical calculations were conducted under the same conditions ( $U_o$ ,  $P$ , and  $2\omega_o$ ) as those used for the experimental measurements. Figure 7a shows trajectories for two particles with the same  $z$ -position and different  $x$ -positions. One particle was injected from the left side of the  $x$ -directional center axis and showed a large retention distance, and the other particle was injected from the right side of the  $x$ -directional center axis and showed a greater retention distance. Figure 7a shows that the retention distances were approximately 60 and 69  $\mu\text{m}$ , respectively. This difference was attributed to a combination of two main factors, i.e., the gradient force and the velocity profile. The retention distance upstream of the laser beam axis was slightly smaller than that downstream of the laser beam axis due to the gradient force, as shown in Fig. 6c. Furthermore, a particle injected from the left side of the microfluidic channel experienced deceleration at a position of higher velocity than the particle injected from the right side. This is clearly shown in Fig. 7b.

under the assumption that  $v = U_o$  (constant) are included for comparison. **c** Trajectories for particles injected into the microfluidic channel at different  $x$ -positions and the same  $z$ -position. **d** Trajectories for particles injected into the microfluidic channel at different  $z$ -positions and the same  $x$ -position

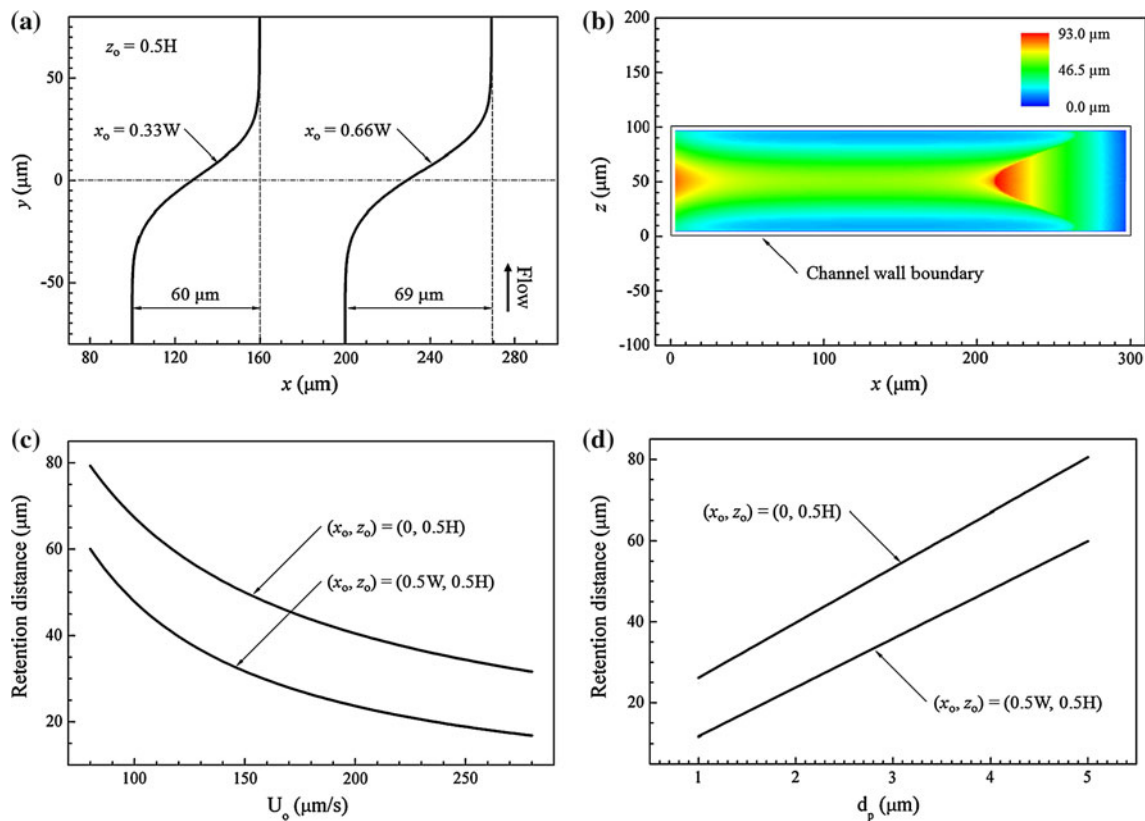


**Fig. 7** Numerical simulation of the particle trajectories ( $\omega_0 = 35 \mu\text{m}$ ,  $P = 1.42 \text{ W}$ ,  $\text{AR} = 3$ ). **a** Two particles with the same  $z$ -position and different  $x$ -positions. **b** Contour of the retention distances for the particles with different  $x$ - and  $z$ -direction injection positions along the cross-section of the microfluidic channel. **c** Retention distances to

the mean velocity by varying the injection positions  $(x_0, z_0) = (0, 0.5H)$  and  $(x_0, z_0) = (0.5W, 0.5H)$ . **d** Retention distances to the particle diameter by varying the injection positions  $(x_0, z_0) = (0, 0.5H)$  and  $(x_0, z_0) = (0.5W, 0.5H)$

Contours of the retention distances for different  $x$ - and  $z$ -positions are shown in Fig. 7b. The retention distance in the microfluidic channel showed bilateral symmetry. However, the axis of symmetry was slightly shifted to the left side of the microfluidic channel due to the aforementioned phenomenon explained in Figs. 6c and 7a. The reduction in the retention distance at the right channel wall arose from collisions between the particle and the channel wall. The hydrodynamic effect was dominant in the lateral direction. The retention distance increased as the injection position moved to the left- and right-hand sides of the channel because the local flow velocity became smaller as the injection position was shifted to the side channel wall. On the other hand, the optical effect was dominant in the vertical direction. The particle injected at the position slightly upper/lower from the center of the channel experienced the same retention distance that injected at the center of the channel due to the increment of the gradient force. Basically, the gradient force increases to the  $y$ - or  $z$ -directional position from the beam center axis and decreases after some critical position (Kim and Kim 2006). The combined effects of the reduction of the local flow

velocity and the increment of the gradient force compensated for the reduction of the scattering force. However, the retention distance became smaller as the vertical distance from the center of the channel and the particle injection position increased, although the local flow velocity became smaller and the gradient force became larger, which led to the longer residence time in an influence region of the laser beam by the reduction of the scattering force. Since the illumination beam had the Gaussian shape, the optical intensity decreased drastically as the particle injection position was shifted to the upper and lower regions of the channel. Therefore, the reduction of the local flow velocity and the increase of the gradient force did not compensate for the decrease of the scattering force, leading to the smaller retention distance. The position that showed the maximum retention distance and ensured an optimal separation resolution lay on the right side of the channel with respect to the  $x$ -direction center axis. Implementation of this system in a practical device revealed that focusing the particle on the right side of the channel had disadvantages, such as collisions between the particle and the channel wall and problems with control over the lateral two sheath flow

rates. For these reasons, the optimal position for achieving separation was found on the left-hand side of the channel.

Figure 7c, d show the retention distances of the different injection positions  $(x_o, z_o) = (0.5W, 0.5H)$  and  $(x_o, z_o) = (0, 0.5H)$  for various particle sizes and mean flow velocities. The resolution of the optical particle separation was related to the flow velocity. Therefore, it could be manipulated using either the flow rate or the particle injection position. As shown in Fig. 7d, the slope of the retention distance as a function of particle size for particles injected at the position  $(x_o, z_o) = (0, 0.5H)$ , i.e., near the left side channel wall region, was slightly larger than it was for particles injected at the center of the channel. The separation resolution was, therefore, higher in the channel wall region. For example, particles with diameters of 1 and 5  $\mu\text{m}$  could be separated 55  $\mu\text{m}$  downstream if they were injected at the position  $(x_o, z_o) = (0, 0.5H)$ . The particles could be separated only 48  $\mu\text{m}$  downstream if they were injected at the position  $(x_o, z_o) = (0.5W, 0.5H)$ . The efficiency of particle separation with injection near the channel wall was approximately 14.5% higher than the efficiency of separation with injection at the center of the microfluidic channel. These results indicate that the resolution of particle separation is influenced by the injection position, even though other adjustable parameters, such as flow rate, laser power, and working fluid properties, remain unchanged.

## 5 Conclusions

The present study examined the optical and hydrodynamic characteristics of the particle motion during a cross-type optical particle separation (COPS) system. The effects of the non-uniform flow velocity profile as well as the optical property on the characteristics of particle behavior were scrutinized. The  $\mu$ -DDPIV method was employed to measure the retention distance in three dimensions. Experimental results showed that the actual retention distance was smaller than the retention distance predicted under the assumption that  $v = U_o$  (constant). This resulted from the reduced residence time in the vicinity of the optical force. The theoretical predictions supported the experimental results well. The gradient force of the laser beam yielded different retention distances upstream and downstream of the laser beam axis. As the  $z$ -position of the particle moved away from the  $z$ -directional center axis, the retention distance decreased due to the decline in the scattering force despite of the increment of the gradient force. By controlling the position of the particle injection, the resolution of the optical particle separation could be manipulated without modifying the flow rate, laser power, or working fluid properties. The present numerical results showed that the retention distance is higher at the left- and right-hand

sides of the channel, but lower at the upper and lower regions of the channel. Nevertheless, the particle focusing to the right-hand side of the channel is not good because the probability of the particle collision to the channel wall is increased, and the particle focusing to the desirable position via the balance between two lateral sheath flows is difficult to control. Thus, the left-hand side of the channel is the best. To make the actual COPS system, it is necessary to focus the particle three-dimensionally. The vertical particle focusing to the center of the channel and the lateral particle focusing to the left channel wall can be accomplished by using the microcapillary with single sheath fluid or simple flow focusing microstructure. Through the results, evaluation of the particle behavior during a cross-type optical particle separation system was established and these results can be applied to the design of actual device.

**Acknowledgments** This work was supported by the Creative Research Initiatives (No. 2011-0000423) program of the National Research Foundation of Korea.

## References

- Ashkin A (1970) Acceleration and trapping of particles by radiation pressure. *Phys Rev Lett* 24:156–159
- Bruus H (2008) *Theoretical microfluidics*. Oxford University Press, New York
- Carlo DD, Irimia D, Tompkins RG, Toner M (2007) Continuous inertial focusing, ordering, and separation of particles in microchannels. *Proc Natl Acad Sci USA* 104:18892–18897
- Chang C-C, Huang Z-X, Yang R-J (2007) Three-dimensional hydrodynamic focusing in two-layer polydimethylsiloxane (PDMS) microchannels. *J Micromech Microeng* 17:1479–1486
- Dholakia K, Reece P, Gu M (2008) Optical micromanipulation. *Chem Soc Rev* 37:42–55
- Fuerstman MJ, Lai A, Thurlow ME, Shevkoplyas SS, Stone HA, Whitesides GM (2007) The pressure drop along rectangular microchannels containing bubbles. *Lab Chip* 7:1479–1489
- Gomez FA (2008) *Biological applications of microfluidics*. Wiley, New Jersey
- Hakem IF, Leech AM, Johnson JD, Donahue SJ, Walker JP, Bockstaller MR (2010) Understanding ligand distribution in modified particle and particle like systems. *J Am Chem Soc* 132:16593–16598
- Hart SJ, Terray AV (2003) Refractive-index-driven separation of colloidal polymer particles using optical chromatography. *Appl Phys Lett* 83:5316–5318
- Helmbrecht C, Niessner R, Haisch C (2007) Photophoretic velocimetry for colloid characterization and separation in a cross-flow setup. *Anal Chem* 79:7097–7103
- Hoi S-K, Udalagama C, Sow C-H, Watt F, Bettiol AA (2009) Microfluidic sorting system based on optical force switching. *Appl Phys B* 97:859–865
- Hoi S-K, Hu Z-B, Yan Y, Sow C-H, Bettiol AA (2010) A microfluidic device with integrated optics for microparticle switching. *Appl Phys Lett* 97:183501
- Hsu H-Y, Ohta AT, Chiou P-Y, Jamshidi A, Neale SL, Wu MC (2010) Phototransistor-based optoelectronic tweezers for dynamic cell manipulation in cell culture media. *Lab Chip* 10:165–172



- Kim SB, Kim SS (2006) Radiation forces on spheres in loosely focused Gaussian beam: ray-optics regime. *J Opt Soc Am B* 23:897–903
- Kim YW, Yoo JY (2009) Axisymmetric flow focusing of particles in a single microchannel. *Lab Chip* 9:1043–1045
- Kim SB, Kim JH, Kim SS (2006) Theoretical development of in situ optical particle separator: cross-type optical particle chromatography. *Appl Opt* 45:6919–6924
- Kim SB, Jung E, Sung HJ, Kim SS (2008a) Optical mobility in cross-type optical particle separation. *Appl Phys Lett* 93:044103
- Kim SB, Yoon SY, Sung HJ, Kim SS (2008b) Cross-type optical particle separation in a microchannel. *Anal Chem* 80:2628–2630
- Kinoshita H, Kaneda S, Fujii T, Oshima M (2007) Three-dimensional measurement and visualization of internal flow of a moving droplet using confocal micro-PIV. *Lab Chip* 7:338–346
- Kuhn S, Measor P, Lunt EJ, Philips BS, Deamer DW, Hawkins AR, Schmidt H (2009) Loss-based optical trap for on-chip particle analysis. *Lab Chip* 9:2212–2216
- Ladavac K, Kasza K, Grier DG (2004) Sorting mesoscopic objects with periodic potential landscapes: optical fractionation. *Phys Rev E* 70:010901
- Lee KH, Kim SB, Lee KS, Sung HJ (2011) Enhancement by optical force of separation in pinched flow fractionation. *Lab Chip* 11:354–357
- MacDonald MP, Spalding GC, Dholakia K (2003) Microfluidic sorting in an optical lattice. *Nature* 426:421–424
- Mao X, Lin S-CS, Dong C, Huang TJ (2009) Single-layer planar on-chip flow cytometer using microfluidic drifting based three-dimensional (3D) hydrodynamic focusing. *Lab Chip* 9:1583–1589
- Maruyama H, Kotani K, Masuda T, Honda A, Takahata T, Arai F (2011) Nanomanipulation of single influenza virus using dielectrophoretic concentration and optical tweezers for single virus infection to a specific cell on a microfluidic chip. *Microfluid Nanofluid* 10:1109–1117
- Ohshima H, Kondo T (1989) Approximate analytical expression for the electrophoretic mobility of colloidal particles with surface-charge layers. *J Colloid Interface Sci* 130:281–282
- Pamme N, Manz A (2004) On-chip free-flow magnetophoresis: continuous flow separation of magnetic particles and agglomerates. *Anal Chem* 76:7250–7256
- Park JS, Kihm KD (2006) Three-dimensional micro-PTV using deconvolution microscopy. *Exp Fluids* 40:491–499
- Psaltis D, Quake SR, Yang C (2006) Developing optofluidic technology through the fusion of microfluidics and optics. *Nature* 442:381–386
- Tsai C-H, Hou H-H, Fu L-M (2008) An optimal three-dimensional focusing technique for micro-flow cytometers. *Microfluid Nanofluid* 5:827–836
- Wang MM, Tu E, Raymond DE, Yang JM, Zhang H, Hagen N, Dees B, Mercer WM, Forster AH, Kariv I, Marchand PJ, Butler WF (2005) Microfluidic sorting of mammalian cells by optical force switching. *Nat Biotechnol* 23:83–87
- Wu M, Robert JW, Buckley M (2005) Three-dimensional fluorescent particle tracking at micron-scale using a single camera. *Exp Fluids* 38:461–465
- Yamada M, Nakashima M, Seki M (2004) Pinched flow fractionation: continuous size separation of particles utilizing a laminar flow profile in a pinched microchannel. *Anal Chem* 76:5465–5471
- Yang AHJ, Moore SD, Schmidt BS, Klug M, Lipson M, Erickson D (2009) Optical manipulation of nanoparticles and biomolecules in sub-wavelength slot waveguides. *Nature* 457:71–75
- Yoon SY, Kim KC (2006) 3D particle position and 3D velocity field measurement in a microvolume via the defocusing concept. *Meas Sci Technol* 17:2897–2905
- Yoon SY, Kihm KD, Kim KC (2011) Correlation of fluid refractive index with calibration coefficient for micro-defocusing digital particle image velocimetry. *Meas Sci Technol* 22:037001
- Yu C, Vykoukal J, Vykoukal DM, Schwartz JA, Shi L, Gascoyne PRC (2005) A three-dimensional dielectrophoretic particle focusing channel for microcytometry applications. *J Microelectromech Syst* 14:480–487